Two Diamine Schiff Base as a Corrosion Inhibitors for Carbon Steel in Sulfuric Acid Solution: Electrochemical Assessment and Theoretical Calculation

Zesheng Chen[1], Zheng Liu[1,*] , Kun-Huan He[2], Guo-Cheng Han[3,*], Yiju Lv [1], Jiaxing Han[1], Xianmei Wei[1]

[1] College of Chemical and Biological Engineering, Guilin University of Technology, Guangxi Key Laboratory of Electrochemical and Magneto-chemical Functional Materials, Guilin 541004, P.R.China
[2] College of petroleum and chemical engineering, Beibu Gulf University, qinzhou 535011, P.R.China
[3] School of Life and Environmental Sciences, Guilin University of Electronic Technology, Guilin, 541004, P.R.China
[*]E-mail: lisa4.6@163.com (Z. Liu); hangc1981@163.com (G.-C. Han).

In this paper, two new bis-Schiff bases corrosion inhibitors, including $N^1E,N^2E-(N^1,N^2)$-(bis(2-hydroxy-5-fluorobenzylidene))propane-1,2-diamine (L1) and (2E,2'E)-2,2'-(pyridine-2,6-diylbis (azanylylidene)) diacetic acid (L2) were synthesized and characterized by IR, UV, MS and ^{1}H-NMR. The purpose of this article is to explore the effect of two corrosion inhibitors on carbon steel in 1 mol/L sulfuric acid. The corrosion inhibition effect of L1 and L2 on carbon steel in sulfuric acid solution was determined by the weightlessness method, electrochemical method, scanning electron microscope, determination of adsorption isotherm and calculation of thermodynamic parameters and quantum chemistry calculations. The results indicated that both inhibitors had good resistance to 1.0 $mol·L^{-1}$ sulfuric acid corrosion and at 30 °C, the corrosion inhibition rates of L1 and L2 were 74.76% and 96.96%, respectively. Scanning electron microscopy, isothermal adsorption equation measurement and quantum chemical calculations indicated that both L1 and L2 were mixed corrosion inhibitors, which can be adsorbed on the surface of carbon steel to form a corrosion inhibitor film. The process of adsorption of Schiff base corrosion inhibitors on carbon steel surface was spontaneous.

1. INTRODUCTION

Carbon steel refers to iron-carbon alloys with a carbon content of less than 2% and a small amount of impurities such as silicon, manganese, and phosphorus and sulfur [1]. Since the industrial revolution of the 18th century, there has been an increasing global demand for carbon steel as a raw

Int. J. Electrochem. Sci., 16 (**2021**) Article ID: 210559

2

material for various products and structures, including buildings, vehicles, electronic equipment, pipes and household appliances. Carbon steel inevitably forms a rust layer in daily transportation, hot rolling, surface treatment, operation and storage. At the same time, steel rolling in the steel industry requires pickling to remove iron oxide scale and other dirt on the steel surface, and the pickling process is pickled. The end point cannot be determined, so it is easy to cause "over-pickling" [2]. Corrosion inhibitors are anti-corrosion chemicals that which can significantly reduce the corrosion rate of metals by adding a small amount material to the environmental medium. Compared with other anti-corrosion methods, corrosion inhibitors are easy to use, economical and effective, and are widely used in industrial production and social life. The Schiff base compound contains N, O, S heteroatoms and unsaturated C=N bonds, which form a strong and stable corrosion-inhibiting adsorption film on the metal surface in the solution, thereby slowing the corrosion of the corrosive liquid on the metal. At the same time, Schiff base has the characteristics of low cost, easy synthesis and purification, good water solubility, no toxicity, which is favored by corrosion inhibitor researchers [3-5]. The diamine double Schiff base corrosion inhibitor synthesized contains more coordination atoms and various coordination forms in the molecular structure [6], which can effectively form a corrosion inhibition film on the surface of carbon steel to achieve good sustained release. The effect is very promising. Other researchers have also conducted a number of studies on the corrosion inhibition properties of Schiff base compounds.

Khan and co-workers synthesized 3-(5-methoxy-2-hydroxybenzylideneamino) -2-(-5-methoxy-2-hydroxyphenyl)-2,3-dihydroquinazoline-4(1H)-one (MMDQ) and 3-(5-nitro-2-hydroxybenzylideneamino)-2(5-nitro-2-hydroxyphenyl)-2,3-dihydroquinazoline-4(1H)-one (NNDQ) Schiff base corrosion inhibitors by Aminobenzyhydrazide, Aromatic salicyaldehyde and 2-hydroxy-5-methoxy benzaldehyde. The weight loss method and electrochemical test results showed that the two corrosion inhibitors had excellent corrosion inhibition performance for carbon steel in the corrosive environment of 1M hydrochloric acid. When the corrosion inhibitor was added at 1 mM, the inhibition rates of MMDQ and NNDQ reached 92% and 88%, respectively [7].

Meng and co-workers synthesized 3-pyridinecarboxaldehyde-4-phenyl thiosemicarbazide (3-PCPTC) and 4-pyridinecarboxaldehyde-4- phenylthiosemicarbazide (4-PCPTC) Schiff base corrosion inhibitors by 3-Pyridine formaldehyde, 4-pyridine formaldehyde and thiosemicarbazide. The weight loss method and electrochemical test results showed that both corrosion inhibitors have excellent corrosion inhibition performance. In the case of 1 M hydrochloric acid and a corrosion inhibitor addition amount of 1 mM, the inhibition rates of 3-PCPTC and 3-PCPTC were 97% and 95%, respectively. Molecular dynamics simulations showed that both corrosion inhibitor molecules could adsorb to the Fe surface in parallel [8].

Elemike and co-workers [9] synthesized E-N-(2-chlorobenzylidiene)-2- methylaniline Schiff base compound by o-chlorobenzaldehyde and o-toluidine. The polarization curves and AC impedance analysis results show that the compound has excellent corrosion inhibition performance for carbon steel in hydrochloric acid solution. Molecular dynamics simulations and quantum chemical calculations showed that the phenyl rings and the imino group were sufficiently involved in electron distribution within the compound with little contribution from the methyl and chloride attachments.

In this study, N^1E,N^2E-(N^1,N^2)-(bis(2-hydroxy-5-fluorobenzylidene))propane-1,2-diamine (L1) was synthesized by the reaction of 1,2-propylenediamine with 5-fluorosalicylaldehyde, and (2E,2'E)-

2,2'-(pyridine-2,6-diylbis(azanylylidene))diacetic acid (L2) was synthesized by reacting 2,6-diaminopyridine with glyoxylic acid. The structure and confirmation of the two diamine double Schiff bases were carried out by IR, UV, MS and ^{1}H NMR. The inhibition efficiency of two diamine double Schiff base inhibitors at different concentrations was determined by weight loss method, electrochemical methods and scanning electron microscopy, as well as adsorption isotherm curves and thermodynamic parameters were calculated to study the corrosion inhibition and corrosion inhibition of two diamine double Schiff base inhibitors. The theoretical calculations of the two corrosion inhibitors were carried out by quantum chemistry, and the structure-activity relationship between the quantum chemical parameters of the corrosion inhibitor molecules and the corrosion inhibition performance was analyzed.

2. EXPERIMENTAL

2.1. Materials and Methods

A 20# carbon steel coupon of dimensions 3.0×1.0×0.3 cm was used for corrosion studies. Analytical grade concentrated sulfuric acid and distilled water were used to prepare 1 mol·L^{-1} dilute sulfuric acid for corrosion experiments. Before the experiment, the samples were all polished with 400, 800, 1200 mesh metallographic sandpaper, rinsed with distilled water, dehydrated by ultrasonic vibration in absolute ethanol, then degreased by acetone, dried with cold air, and sealed with non-working surface with molten paraffin. The filter paper was wrapped and placed in a desiccator for 4 h. The size was measured before testing and the surface area was determined. The VECTOR22 infrared spectrometer was used to scan the two diamine amines and the preparation materials in the range of 4000-500 cm^{-1} by KBr compression. At room temperature, the corrosion inhibitor was prepared into a solution of 10^{-4} mol·L^{-1} using dichloromethane (DCM) or N, N-dimethyl formamide (DMF) as solvent, and the UV spectrum of the reaction materials and two kinds of binary amine Schiff base were determined by UV-2450 UV-visible spectrophotometer. The prepared binary was prepared by using an AUANCEAv 500Hz superconducting NMR spectrometer with deuterated methylene chloride or deuterated dimethyl sulfoxide or deuterated chloroform with 1.0×10^{-4} mol·L^{-1} corrosion inhibitor as solvent. The amine double Schiff base corrosion inhibitor was tested by nuclear magnetic resonance spectroscopy. Mass spectrometry was performed using a Bruker Solarix XR FTMS Fourier High Resolution Mass Spectrometer. The spectrum of the double Schiff base corrosion inhibitor was obtained by analysis by Bruker Compass Data Analysis 5.0 software.

1,2-propylenediamine, 2,6-diaminopyridine were purchased from Shanghai Macklin Biochemical Co., Ltd. (China). 5-fluorosalicylaldehyde and glyoxylic acid were obtained from Aladdin Reagent Co., Ltd. (Shanghai, China). L1 and L2 were synthesized according to Scheme 1. The yield of L1 was 75.64%, and the yield of L2 was 85.46%.

L1
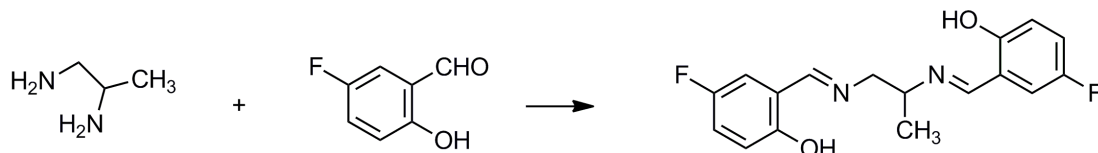
L2
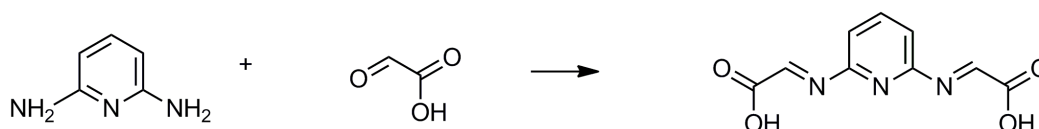
Scheme 1. Synthetic routes for L1 and L2

2.2 Weight Loss Measurement

The carbon steel sample was accurately weighed, and the treated carbon steel sheets were immersed in the non-addition and addition of different concentrations of 0.001×10^{-3}, 0.005×10^{-3}, 0.01×10^{-3} mol·L^{-1} L1 and L2 in 50 mL of 1 mol·L^{-1} dilute sulfuric acid, soaked at 30 °C for 4 h. Then took out the sample, rinsed it with distilled water, dehydrated it in ethanol, degreased in acetone, and weighed it after drying for 4 h [10]. Three parallel experiments were performed, and the average weight loss ΔW(g), corrosion rate (A), surface coverage (θ), corrosion inhibitor corrosion inhibition rate (η_W%) were calculated by the following formula [11,12]:

$$\Delta W = W_0 - W_1 \qquad (1)$$

Where, ΔW(mg) was the mass difference of the carbon steel samples before and after tests, W_0 and W_1 were the average mass of the sample before and after immersion, respectively.

$$A = \frac{\Delta W}{S \times t} \qquad (2)$$

Where, S(cm^2) was the total immersion area of the carbon steel sample, t(h) was the immersion time.

$$\theta = \frac{A^0_{corr} - A_{corr}}{A^0_{corr}} \qquad (3)$$

$$\eta_W\% = \left(\frac{A^0_{corr} - A_{corr}}{A^0_{corr}}\right) \times 100\% \qquad (4)$$

Where, A^0_{corr} and A_{corr} (g·cm^{-2}·h^{-1}) were carbon steel without and containing corrosion inhibitor Corrosion rate in a 1 mol·L^{-1} dilute sulfuric acid solution.

2.3 Electrochemical measurements

The traditional three-electrode system was used, the platinum wire electrode was the counter electrode(CE), the saturated calomel was the reference electrode(RE), the carbon steel was the working

electrode(WE), and the electrochemical tests were performed by the CHI760-E electrochemical workstation.

The electrochemical impedance spectroscopy was carried out at room temperature. Before conducting EIS measurement, the working electrode carbon steel was immersed in the etching solution for 30 min. After the system potential was stabilized, this potential was the open circuit potential. The frequency ranged from 10^5 Hz to 10^{-2} Hz and the sensitivity was automatically adjusted for sensitivity. Selected the appropriate equivalent potential map and used the Zview software to fit the impedance data. The corrosion inhibition rate η_Z (%) was calculated by the following formula:

$$\eta_Z(\%) = \frac{R_{ct} - R_{ct}^0}{R_{ct}} \times 100\% \qquad (5)$$

Where R_{ct} and R^0_{ct} were charge transfer resistors which containing different concentrations of corrosion inhibitors and no corrosion inhibitors.

The potentiodynamic polarization curve was measured at room temperature, and the potentiodynamic polarization curve was measured using a conventional three-electrode system using an electrochemical workstation. The scanning interval was ±1500mV, the scanning rate was 1.0 mV·s^{-1}, the sensitivity was set to automatically adjust the sensitivity, the electrochemical corrosion parameters were measured by CHI760-E software, the corrosion potential E_{corr} (mV / SCE), the cathode and anode Tafel slope β_c And β_a (mV / dec), corrosion current density icorr (η_A cm^{-2}), corrosion inhibition rate η_T (%) were calculated by the following formula:

$$\eta_T = \left(\frac{i_{corr}^0 - i_{corr}}{i_{corr}} \right) \times 100\% \qquad (6)$$

Where, i^0_{corr} and i_{corr} were corrosion current densities of carbon steel electrodes that do not contain and contain different concentrations of corrosion inhibitor in 1.0 mol·L^{-1} dilute sulfuric acid solution.

2.4 Scanning electron microscopy studies

The surface morphology of the carbon steel test piece before and after corrosion was observed by scanning electron microscopy (SEM) and compared with the blank sample. The scanning electron microscope magnification was 1000 times and the acceleration voltage was 5.0 kV.

2.5 Adsorption isotherms and thermodynamic parameters

1.0 mol·L^{-1} dilute sulfuric acid was used as the etching solution, the concentrations of the diamine double Schiff base inhibitors were 0.001×10^{-3}, 0.005×10^{-3}, and 0.01×10^{-3} mol·L^{-1}, respectively, at 20, 30, and 40°C, according to the method of Section 2.2. In the experiment, the corrosion inhibition rate (surface coverage) was obtained. According to the experimental data of weight loss method, the C/θ was plotted on the ordinate and C was plotted on the abscissa to establish the Langmuir adsorption isotherm equation [13]:

$$\frac{C}{\theta} = \frac{1}{K_{ads}} + C \qquad (7)$$

Where, *C* was the corrosion inhibitor concentration; *θ* was the surface coverage, and *K*$_{ads}$ is the adsorption equilibrium constant.

2.6 Quantum chemical calculation

All structural parameter calculations in this section were performed using the Gaussian09 program [14]. The planar structure of the molecule was plotted using Chemdraw Ultra 12.0 software, the optimized molecular structure was drawn using the GaussView5 program, and the quantitative structural relationship model was established using the IBM SPSS Statistics 20 program [15]. All geometric configuration optimization and quantum chemical calculations were performed using the B3LYP \ 6-311 + G(d, p) method. From the 12 structural parameters of corrosion inhibitors, E$_{HOMO}$, E$_{LUMO}$, gap energy ΔE, chemical hardness, chemical softness, dipole moment, electronegativity, and the maximum number of electrons transferred in the chemical reaction were selected for analysis.

Electronegativity (*χ*) was a measure of the ability of an atom or group of atoms to attract electrons toward themselves and is calculated using the following formula [16]:

$$\chi \approx -\frac{1}{2}(E_{HOMO} + E_{LUMO}) \quad (8)$$

Chemical hardness (*η*) measures the resistance of an atom or group of atoms to charge transfer [17], calculated using the following formula:

$$\eta \approx -\frac{1}{2}(E_{HOMO}-E_{LUMO}) \quad (9)$$

Chemical softness (*σ*) describes the ability of an atom or group of atoms to receive electrons [18], calculated using the following formula:

$$\sigma \approx 2/(E_{HOMO}-E_{LUMO}) \quad (10)$$

The maximum number of electrons transferred in a chemical reaction (ΔNmax) is calculated by the following formula [19]:

$$\Delta N_{max} = \frac{\chi}{2\eta} \quad (11)$$

3. RESULTS AND DISCUSSION

3.1 Characterization of L1 and L2

In the infrared spectrum of Figure S1 for L1, the stretching vibration peak of C=N at 1630 cm^{-1}, the stretching vibration peak of 1488 cm^{-1} attributed to the aromatic ring C=C, and the intrinsic bending of 1255 cm^{-1} belonging to the aromatic ring=C-H Vibration absorption peak; while L1 does not exhibit the stretching vibration peak of -NH$_2$ near 3411 cm^{-1}; there is no stretching vibration peak of aldehyde group (-COH) near 1674 cm^{-1}, and a new chemical bond C=N double bond appears, indicating the formation of Schiff base. In the infrared spectrum of Figure S1 for L2, the stretching vibration peak of C=N at 1601 cm^{-1}, the wide peak of 3383 cm^{-1} is attributed to the OH stretching vibration in the adsorbed water, and the stretching vibration attributed to the aromatic ring C=C at 1446 cm^{-1} Peak; there is no stretching vibration peak of -NH$_2$ near 3384 cm^{-1}, no aldehyde group (-COH) stretching vibration peak

is found near 1749 cm^{-1}, and a new chemical bond C=N characteristic absorption peak appears, also indicating the formation of Schiff base. The characteristic peak data of all the above functional groups are basically consistent with the infrared spectrum data reported in the literature [20,21]

The UV-vis spectrum of Figure S2(a) shows that 1,2-propylenediamine in DCM has an absorption peak at 229 nm, and the n-π* transition attributed to -NH$_2$ produces an absorption band; 5-fluorosalicylaldehyde at 229 nm, 253 nm. There is an absorption peak at 340 nm, where 229 nm is the R absorption band of the carbonyl group (C=O) n-π* transition, and 253 nm is the π-π* of the carbonyl group (C=O) conjugated to the benzene ring. The K absorption band generated by the transition, the B absorption band generated by the π-π* transition of the benzene ring at 340 nm; the absorption peak of L1 at 231 nm, 253 nm and 327 nm, respectively assigned to the R absorption band of the n-π* transition of C=N, the K absorption band generated by the π-π* transition of the carbon-nitrogen double bond (C=N) conjugated to the benzene ring, and the B absorption band generated by the π-π* transition of the benzene ring, and compared with the raw materials, the absorption peak position of the ultraviolet absorption spectrum produces a large change, indicating the formation of a new compound [22].

The UV-vis spectrum of Figure S2(b) shows that 2,6-Diaminopyridine in DCM has an absorption peak at 245 nm and 306 nm, where the n-π* transition of -NH$_2$ at 245 nm produces an absorption band, and At 306 nm, it is the B absorption band generated by the π-π* transition of the benzene ring; the glyoxylic acid has an absorption peak at 219 nm, and is assigned to the R absorption band generated by the n-π* transition of the carbonyl group (C=O); L2 has absorption peaks at 246 nm and 320 nm, which are respectively assigned to the R absorption band generated by the n-π* transition of C=N and the B absorption band generated by the π-π* transition of the benzene ring. Compared with the two raw materials, the absorption peak position of the ultraviolet absorption spectrum is compared. Large changes indicate the formation of new compounds [22].

Figure S3 is a nuclear magnetic resonance spectrum of L1. As shown in Figure S3, a doublet peck of two hydrogen atoms of the -CH=N- group at 8.27 ppm; 7.29 ppm is the peak of the hydrogen atom on the carbon adjacent to the hydroxyl group on the benzene ring; a peak of a hydrogen atom on the carbon adjacent to the fluorine atom on the benzene ring at 6.93 ppm; no peak of the hydroxyl group is found at 5.00 ppm, and the hydrogen in the hydroxyl group may be deuterated by the deuterated reagent. At 3.74 ppm, it is the peak of two hydrogen atoms on the C-CH$_2$-N skeleton, at 3.91 ppm, it is the peak of the hydrogen atom on the N-CH-C skeleton; and at 1.43 ppm, it is the peak of the three hydrogen atoms on the methyl group. The solvent deuterated dimethyl sulfoxide peak overlaps with the hydrogen atom peak on the benzene ring adjacent to the hydroxyl group at 7.28 ppm. All the above nuclear magnetic resonance data are basically consistent with the corresponding functional group hydrogen peak data reported in the literature [23-25]

Figure S4 is a mass spectrum of L2. It can be seen from Figure S4 that the quasi-molecular ion peak at [M-2H]$^-$ m/z 219.18 is formed by the loss of two H$^+$ of the test substance L2 through the split, and the relative molecules of the tested substance L2 are estimated. The mass is 221.18, which is basically consistent with the L2 theoretical value 221.04.

3.2. Corrosion Inhibition Studies

3.2.1 Weight Loss Experiments

It can be seen from Table 1 that at the same temperature and under the same corrosion inhibitor, the concentration of the corrosion inhibitor increases and the corrosion rate decreases. This is because the concentration of the corrosion inhibitor increases, resulting in an increase in the surface coverage of the carbon steel, thereby increasing the corrosion inhibition rate of the corrosion inhibitor. The corrosion inhibition rate of L1 reached 74.76% at a concentration of 0.01×10^{-3} mol·L^{-1}. The corrosion inhibition rate of L2 reached 96.96% at a concentration of 0.01×10^{-3} mol·L^{-1}. The reason why the corrosion inhibition performance of L2 is better than that of L1 is related to the fact that it contains a plurality of coordinating nitrogen atoms with large electronegativity. More points will produce multiple adsorption points, and the conjugated system in the molecular structure is larger, which can form a dense coating on the surface of carbon steel to reduce corrosion [14].

Table 1. Corrosion parameters of carbon steel samples immersed in 1 mol·L^{-1} dilute sulfuric acid solution containing L1, L2 at different concentrations for 4 h at 30 °C

Inhibitor	C(mM)	ΔW(g)	k (g·cm^{-2}· h$^{-1)}$)	θ	ηw%
Blank	-	0.9525	0.07938	-	-
	0.001	0.5107	0.04256	0.6775	67.75
L1	0.005	0.2833	0.02361	0.7025	70.25
	0.01	0.2404	0.02003	0.7476	74.76
	0.001	0.0925	0.00771	0.9028	90.28
L2	0.005	0.0466	0.00247	0.9511	95.11
	0.01	0.027 7	0.00241	0.9696	96.96

3.2.2 Potentiodynamic polarization

It can be seen from Figure 1 that the E_{corr} value of the corrosion inhibitor sample is not changed much compared with the blank sample E_{corr} value, and the absolute value difference is less than 85 mV, indicating that the two corrosion inhibitors (L1, L2) are mixed type corrosion inhibitor [26]. The mixed corrosion inhibitor can simultaneously suppress the anode metal dissolution reaction and the cathode reduction hydrogen evolution reaction occurring in the corrosion reaction. It can be seen from Figure 1 that after the addition of the corrosion inhibitor, the polarization curve moves downward, the corrosion current decreases, and the inhibition rate increases [27], and with the higher concentration of corrosion inhibitor added, the more the corrosion current is reduced.
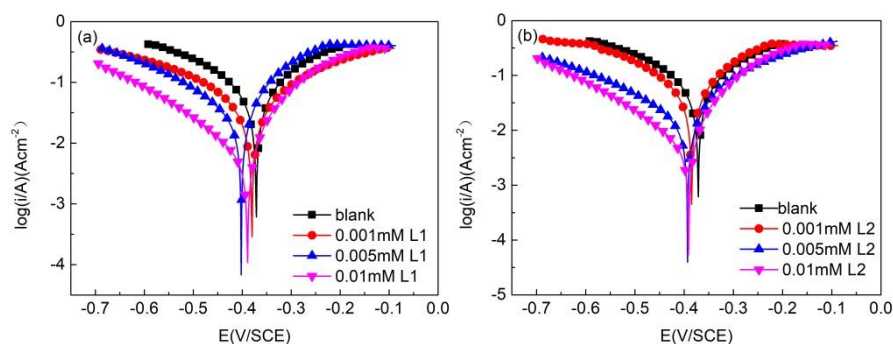
Figure 1. Polarization plot of carbon steel in a 1.0 mol·L^{-1} dilute sulfuric acid solution in absence and presence different concentrations of L1(a) and L2(b)

It can be seen from Table 2 that after the addition of the corrosion inhibitor, as the concentration of the corrosion inhibitor increases, the corrosion current density decreases, and the corrosion inhibition rate increases. The highest corrosion inhibition efficiency of L1 is 87%, and the highest corrosion inhibition efficiency of L2 is 88.9%. This may be due to an increase in the concentration of the Schiff base inhibitor resulting in an increase in the surface coverage of the corrosion inhibitor. Compared with the blank sample, the Tafel constants β_c and β_a values did not change much, it is indicated that the corrosion inhibitor molecules reduce the reactive sites by adsorbing on the surface of the carbon steel to form an adsorption film layer, thereby inhibiting corrosion.

Table 2. Electrochemical corrosion parameters of carbon steel in 1.0 mol·l^{-1} dilute sulfuric acid solution containing different concentrations of schiff base corrosion inhibitor

inhibitor	C (mM)	-E_{corr} (mV/sce)	-β_c (mV/dec)	β_a (mV/dec)	i_{corr} (μAcm^{-2})	η_T (%)
blank		371	51	54	788	-
L1	0.001	380	51	54	420	46.7
	0.005	402	54	64	405	48.6
	0.01	389	64	80	102	87
L2	0.001	384	54	62	591	25
	0.005	393	53	64	215	72.7
	0.01	391	64	85	87	88.9

3.2.3 Electrochemical Impedance Spectroscopy (EIS)

Figure 2 is an electrochemical impedance diagram (Nyquist diagram) of carbon steel in a 1.0 mol·L^{-1} dilute sulfuric acid solution containing no corrosion inhibitor and containing different concentrations of L1 and L2 Schiff base corrosion inhibitors. Figure 3 is a Bode curves carbon steel in a 1mol·L^{-1} dilute sulfuric acid solution in absence and presence different concentrations of L1and L2. Figure 4 is an equivalent circuit diagram of impedance spectrum data fitting, R^0_P is the polarization

resistance of carbon steel in the case where no corrosion inhibitor is added, which is equal to the sum of the charge transfer resistance R_{ct} and the diffusion layer resistance R_d; After the addition of the corrosion inhibitor, R_p is the sum of R_p, film resistance R_f and accumulated species R_a; R_s is the solution resistance [28].
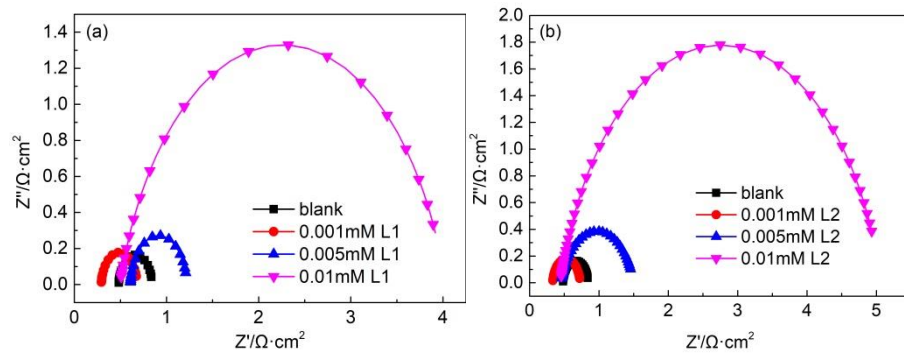
Figure 2. Nyquist diagram of carbon steel in a 1.0 mol·L^{-1} dilute sulfuric acid solution in absence and presence different concentrations of L1(a) and L2(b)
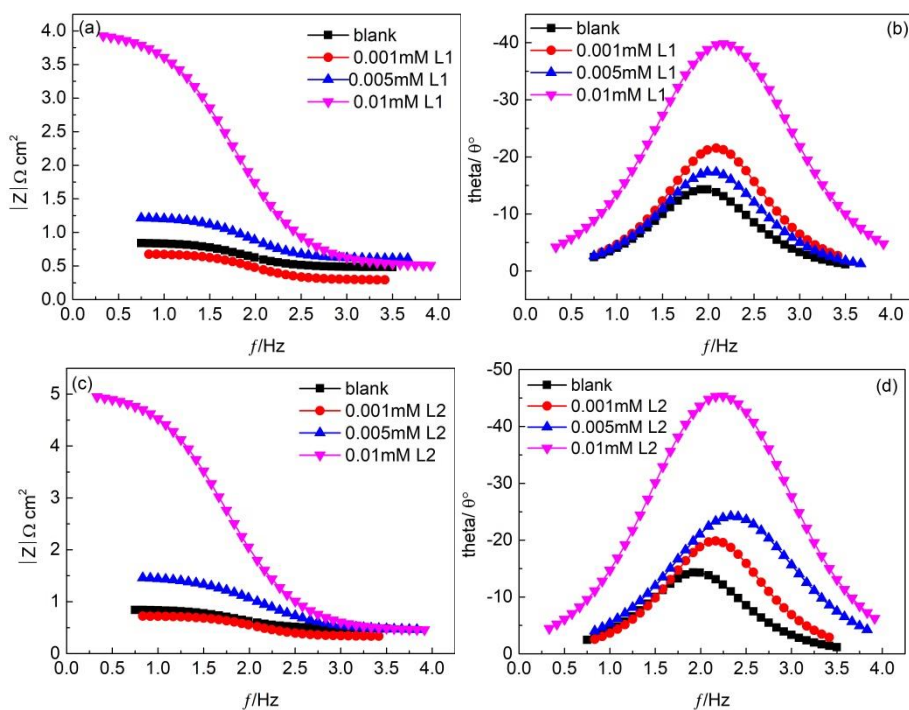
Figure 3. The Bode curves carbon steel in a 1.0 mol·L^{-1} dilute sulfuric acid solution in absence and presence different concentrations of L1(a) , (b)and L2(c),(d)
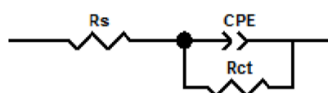
Figure 4. The equivalent circuit diagram

In order to better fit the impedance data of the system, the constant phase element CPE was introduced into the double layer capacitor C_{dl}. Since the interface between the carbon steel and the solution was not an ideal capacitance, the impedance of the CPE was calculated by the following formula [29]:

$$Z_{CPE} = [Y_0(j\omega)^n]^{-1} \qquad (12)$$

Where, Y_0 is the proportionality coefficient of CPE, j is the imaginary number ($j^2 = -1$), ω is the angular frequency ($\omega = 2\pi f$) and n is the phase shift; C_{dl} is calculated by the following formula [30]:

$$C_{dl} = Y_0(\omega''m)^{n-1} \qquad (13)$$

Where, ω'' is the angular frequency at the maximum value for imaginary part of the impedance Z'' ($\omega''m = 2\pi f_{max}$).

It can be seen from Figure 2 that the Nyquist curve of carbon steel in a 1 mol·L^{-1} dilute sulfuric acid solution containing no corrosion inhibitor and a different concentration of Schiff base corrosion inhibitor exhibits a single separation of the capacitive reactance arc. Due to the surface roughness of carbon steel, impurities, dislocations, grain boundaries, as well as the adsorption of corrosion inhibitors, the formation of porous layers and the unevenness of the electrode surface, the Nyquist and ideal circular shape measured deviates from the ideal perfect circle shape, this phenomenon is often referred to as the frequency dispersion of the interface impedance [31]. The addition of corrosion inhibitor significantly changes the radius of the capacitive reactance arc, and the radius of the capacitive anti-arc increases with the increase of the corrosion inhibitor concentration. The reason is that after the corrosion inhibitor is added, a protective film is formed at the interface of the carbon steel/acid medium [32-35], causing the charge transfer resistance to increase and the corrosion to decrease.

Table 3. Impedance spectral parameters of carbon steel in 1.0 mol·l^{-1} dilute sulfuric acid solution containing different concentrations of L1 and L2

| inhibitor | C(mM) | Rs(Ωcm^{-2}) | R$_{ct}$(Ωcm^{-2}) | CPE | | C$_{dl}$(×10^{-6}s^n·Ω^{-1}·cm^{-2}) | η$_z$(%) |
				Y$_0$(×10^{-6}s^n·Ω^{-1}·cm^{-2})	n		
blank	-	0.4815	0.36555	0.010088	0.93014	0.006607	-
L1	0.001	0.29229	0.39019	0.007085	0.94066	0.004889	6.31
	0.005	0.60678	0.61746	0.005741	0.91944	0.003524	40.80
	0.01	0.4958	3.529	0.002984	0.82238	0.001127	89.64
L2	0.001	0.33337	0.39282	0.006252	0.94076	0.004318	6.94
	0.005	0.44922	1.05	0.005081	0.80541	0.001457	65.19
	0.01	0.4424	4.647	0.002234	0.83462	0.000902	92.13

It can be seen from Table 3 that as the concentration of the corrosion inhibitor increases, the charge transfer resistance (R$_{ct}$) increases and the corrosion inhibition rate increases. When the concentration of corrosion inhibitors L1 and L2 was 0.01×10^{-3}mol·L^{-1}, the corrosion inhibition rates of L1 and L2 are 89.64% and 92.13%, respectively. The electrochemical impedance data show that the corrosion inhibitor L2 has better corrosion inhibition performance than L1, which is consistent with the results of the polarization curve and the weight loss method.

3.2.4 Adsorption isotherms and thermodynamic parameters

The adsorption isotherm is considered to be a curve describing the interaction between the corrosion inhibitor molecule and the metal surface active site [36]. The adsorption isotherm model includes the Fumkin adsorption isotherm [37], the Temkin adsorption isotherm [38], the Freundlich standard isotherm [39], the Floy-Huggins [40] and the Langmuir adsorption isotherm [41]. The Langmuir adsorption isotherm is the most commonly used adsorption model, which assumes that the solid surface contains a fixed number of adsorption sites, one for each site [42]. As shown in Figure 5(a) and (b), $C/\theta \sim C$ shows a straight line trend, and the slopes of L1 and L2 are close to 1, indicating that the Langmuir adsorption model is the best fit model for describing this study [43]. The adsorption equilibrium constant at different temperatures can be obtained by Langmuir adsorption isotherm.
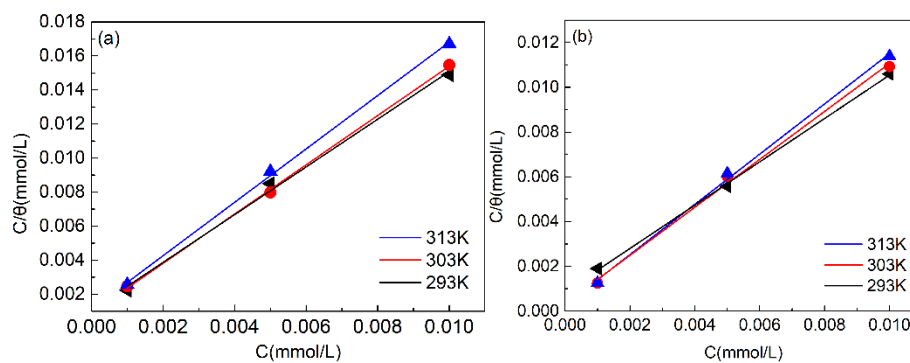

Figure 5. Langmuir adsorption isotherm model of L1(a) and L2(b) on carbon steel surface

Table 4. Thermodynamic parameters of carbon steel in 1.0 mol·L^{-1} dilute sulfuric acid solution containing different concentrations of L1 and L2 at different temperatures

inhibitor	T	r^2	Slope	K_{ads}	ΔG^0_{ads}	ΔH^0_{ads}	ΔS^0_{ads}
	(K)			(L·mol^{-1})	(KJ·mol^{-1})	(KJ·mol^{-1})	(JK^{-1} mol^{-1})
L1	293	0.9931	1.4013	813.01	-26.1	-8.570	118.4
	303	0.9988	1.4477	684.93	-25.7		113.1
	313	0.9983	1.5682	641.02	-25.5		108.9
L2	293	0.9987	0.9682	1381.0	-28.4	-44.98	250.4
	303	0.9938	1.0717	995.7	-27.5		239.2
	313	0.9961	1.1223	704.2	-27.5		231.6

According to the Langmuir adsorption isotherm, a series of thermodynamic parameters can be obtained, such as the standard Gibbs free energy change ΔG^0_{ads}, the enthalpy change ΔH^0_{ads} and the entropy change ΔS^0_{ads}. These thermodynamic parameters can be calculated according to the following formulas. The calculation results are shown in Table 4.

$$K_{ads} = \frac{1}{55.5} exp(-\frac{\Delta G^0_{ads}}{RT}) \qquad (14)$$

$$lnK_{ads} = \frac{\Delta H^0_{ads}}{RT} + constant \qquad (15)$$

$$\Delta G^0_{ads} = \Delta H^0_{ads} - T\Delta S^0_{ads} \qquad (16)$$

The ideal gas constant R is $8.3144 \cdot J \cdot K^{-1} \cdot mol^{-1}$, the temperature T is the thermodynamic temperature, and the value of 55.5 is the molar concentration of water ($mol \cdot L^{-1}$).

It can be seen from the data in Table 4 that the value of the adsorption equilibrium constant K_{ads} decreases gradually at 20 °C, 30 °C, 40 °C, which indicates that the temperature increase is not conducive to the diamine double Schiff base inhibitor in dilute sulfuric acid solution.

The larger the adsorption equilibrium constant K_{ads} value, the more strongly the corrosion inhibitor molecules are adsorbed on the surface of carbon steel, and the adsorption is stronger, and the corrosion is more difficult to occur. When L2 is 293K, the K_{ads} value is the highest, which is 1381 $L \cdot mol^{-1}$. When L1 is 293K, the K_{ads} value is the highest, which is 831.01 $L \cdot mol^{-1}$, indicating that L2 has strong adsorption capacity and better corrosion inhibition ability than L1. According to the literature [44], when the absolute value of the Gibbs free energy ΔG^0_{ads} change of the corrosion inhibitor adsorption process is lower than 20 $kJ \cdot mol^{-1}$, the adsorption at this time belongs to physical adsorption, and the adsorption force is The electrostatic attraction of the corrosion inhibitor molecule and the surface of the carbon steel; When the absolute value of the Gibbs free energy change ΔG^0_{ads} of the corrosion inhibitor adsorption process is higher than 40 $kJ \, mol^{-1}$, the adsorption at this time belongs to chemical adsorption, and the adsorption force is that the corrosion inhibitor molecule forms covalent bond with the metal atom through transferring charge. The data in Table 4 shows that the absolute value of Gibbs free energy change ΔG^0_{ads} of Schiff base corrosion inhibitors L1 and L2 is between 20-40 $kJ \, mol^{-1}$ under three temperature gradients, which indicates that The adsorption process of the etchant on the surface of carbon steel may involve complex interactions, which work together for physical adsorption and chemical adsorption. ΔG^0_{ads} is a negative value, indicating that the adsorption of Schiff base inhibitor molecules on the surface of carbon steel is spontaneous. The negative value of ΔH^0_{ads} indicates that the adsorption is an exothermic process, so the temperature rises and the adsorption is not easy. Table 4 also shows that the adsorption process entropy of the corrosion inhibitor is positive. This is because the corrosion inhibitor molecules are adsorbed on the surface of carbon steel, which is an entropy reduction process. The desorption of adsorbed water on the surface of carbon steel is an entropy increase process. Since the molecular weight of the double Schiff base corrosion inhibitor is much larger than that of water molecules, one When the corrosion inhibitor adsorbs on the surface of the carbon steel, a plurality of water molecules are desorbed, so the whole adsorption process exhibits an entropy increase process.3.2.6 Scanning Electron Microscopic

Figure 6 show SEM images of carbon steel in a steel containing no corrosion inhibitor and containing different concentrations of L1 and L2 Schiff base corrosion inhibitor in 1 $mol \cdot L^{-1}$ dilute sulfuric acid solution. It can be seen that in the dilute sulfuric acid etching solution without corrosion

inhibitor, the surface of the carbon steel is severely corroded, the surface is uneven, there is a serious pit shape, the surface structure is relaxed, and more crystal grain corrosion products are formed.
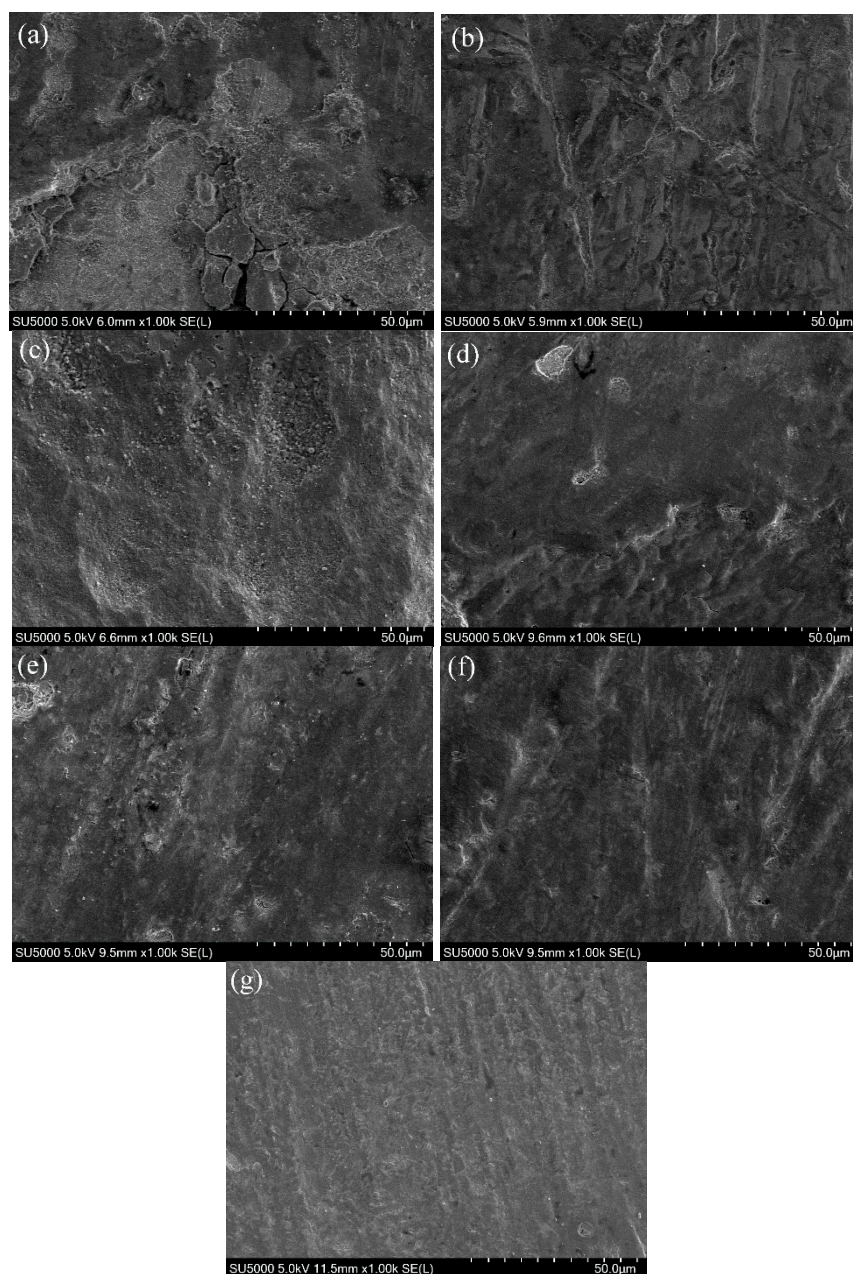

Figure 6. Surface topography of carbon steel after soaking for 4 h in 1.0 mol·L^{-1} dilute sulfuric acid solution of absence(a), presence of 0.001(b), 0.005(c), 0.01 ×10^{-3}(d)mol·L^{-1} L1 and presence of 0.001(e), 0.005(f), 0.01 ×10^{-3} (g)mol·L^{-1} L2

With the increase of corrosion inhibitor concentration, the corrosion degree of carbon steel surface is getting smaller and smaller, and the surface of carbon steel is more and more flat. Especially, when the concentration of corrosion inhibitor is 0.01×10^{-3} mol·L^{-1}, the surface of carbon steel is good. Protection, this is because the corrosion inhibitor molecules form a tight protective film on the surface

of carbon steel, even after soaking for 4h in 1 mol·L^{-1} dilute sulfuric acid solution at 40°C, the surface is basically flat, showing L2 has excellent corrosion inhibition performance in 1 mol·L^{-1} dilute sulfuric acid. Although the corrosion inhibition effect of L1 is not good, L1 also has a good inhibitory effect on carbon steel corrosion.

3.2.5 Quantum chemical calculation

(1)Schematic diagram of Schiff base L1, L2

Figure 7 is a schematic diagram showing the geometric structure of the double Schiff base corrosion inhibitors L1(a) and L2(b). It can be seen from the molecular structure of L1 that the two aromatic rings are not coplanar with the C=N-CH$_2$-HC(CH$_3$)-N=C chain, which is related to the fact that the segment contains a free-spinning σ single bond, plus an intermediate carbon. With a methyl group attached, there is a certain steric hindrance, making the segment difficult to coplane with the two benzene rings. L2 has better coplanarity than L1, and the pyridine ring is coplanar with C=N on both sides.
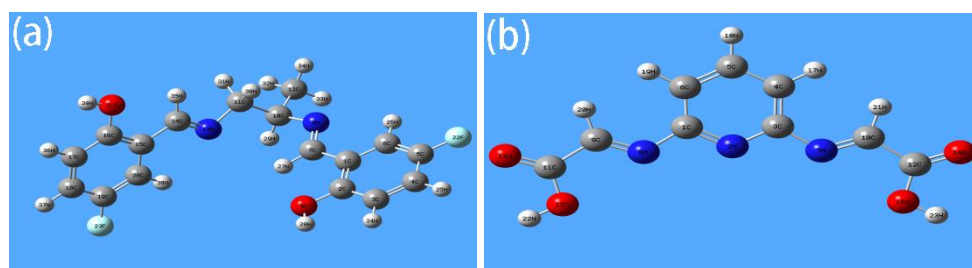

Figure 7. Schematic diagram of protonated structure and planar structure after L1(a) L2(b) optimization; (2) HOMO, LUMO diagram of Schiff base L1, L2

From Figure 8 and Figure 9, the arrangement of HOMO and LUMO orbitals of all atoms can be seen. The highest occupied orbital energy of a molecule E$_{HOMO}$, is a measure of the electron-donating ability of a molecule. The higher the orbital energy is, the more unstable the electrons in the orbit are, and the stronger the electron-donating ability is. The lower the lowest empty orbital energy E$_{LUMO}$ of the molecule, the easier it is for the molecule to accept external electrons [45]. The gap energy ΔE indicates the reactivity of the molecule under study, and molecules with smaller ΔE values are more reactive than molecules with large ΔE values [46]. Figure 8 and Figure 9 show that in the L1 molecular structure, the highest occupied orbital, the lowest empty orbital energy is mainly distributed in two benzene rings and two C=N, C=N-CH$_2$-HC(CH$_3$)-N=C The intermediate carbon and its attached -CH$_3$ are less distributed. Two benzene rings and two C=N are the active sites of the corrosion inhibitor L1, that is, the highest occupied orbital in the molecular structure can provide electrons to form coordination bonds with metallic iron, and the lowest empty orbit can accept electrons of metallic iron. A feedback button is formed to cause the corrosion inhibitor to adsorb on the metal surface to form an adsorption corrosion-inhibiting film layer. In the molecular structure of L2, the highest occupied orbital is mainly distributed

Int. J. Electrochem. Sci., 16 **(2021)** Article ID: 210559

16

on the pyridine ring and two C=N, and the lowest empty orbit is mainly distributed on the pyridine ring, two C=N and carboxyl groups, and these groups will become the active sites of L2, interacting with metallic iron through a coordination or feedback bond to become an adsorption center.
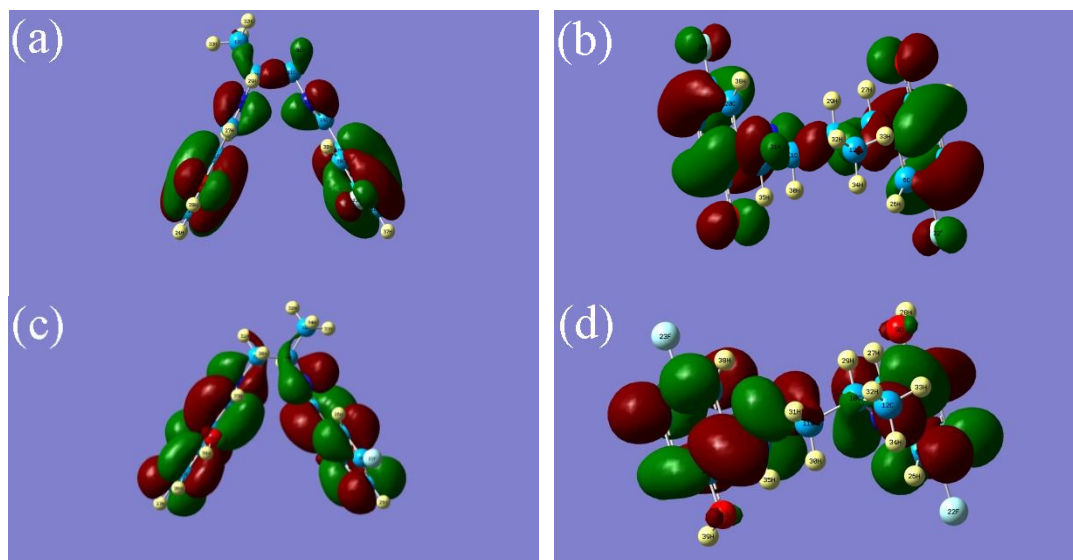

Figure 8. HOMO (a: front view; b: top view) and LUMO diagram(c: front view; d: top view) of Schiff base L1
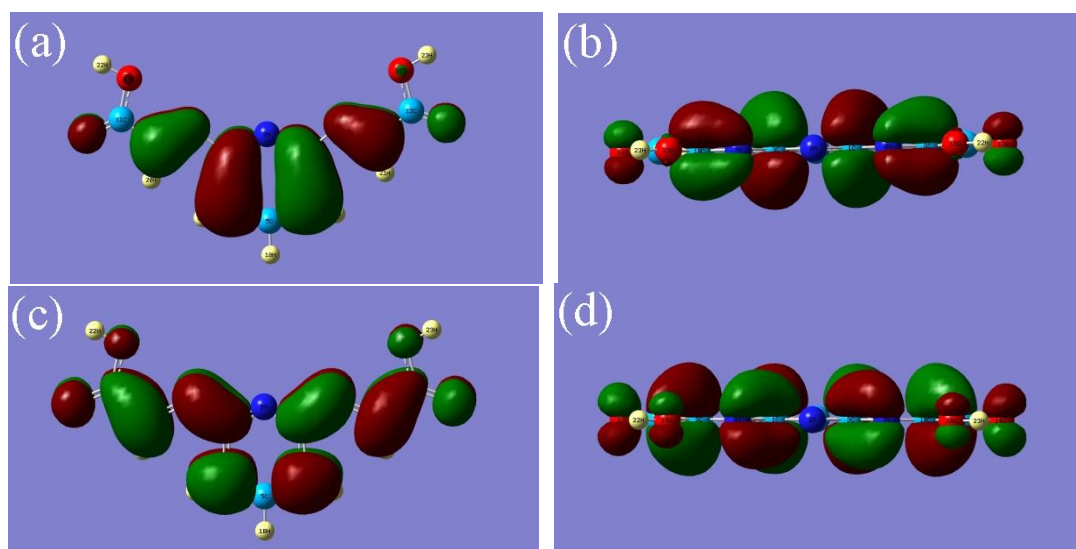

Figure 9. HOMO (a: front view; b: top view) and LUMO diagram(c: front view; d: top view) of Schiff base L2

(3) Correlation analysis between structural parameters and corrosion inhibition efficiency

The molecular structural parameters of L1 and L2 are listed in Table 5. It is well known that the absolute value of the gap energy is small, indicating that the corrosion inhibitor is easy to give the

combination of electrons and metal iron to form a corrosion-inhibiting film layer, which produces better corrosion inhibition. The gap energy shown in Table 5 is ΔE L1>L2. Note L2 is better than L1 for corrosion inhibition. This is consistent with the experimental results.

The dipole moment μ is a measure of the polarity of the covalent bond and is related to the distribution of electrons in the molecule. Usually a large μ value is beneficial to the adsorption of the corrosion inhibitor on the metal surface. As shown in Table 5, the dipole moment μ values of L1 and L2 are both large. This is related to the fact that the L1 structure contains a fluorine atom with a large electronegativity, which increases the polarity of the molecule and a carboxyl group having a strong electron-withdrawing ability in the L2 structure. Both L1 and L2 showed a high corrosion inhibition rate, which is consistent with the experimental results.

The trend of chemical softness (σ) is L2 > L1, the trend of chemical hardness (η) is L1 > L2, and the trend of chemical hardness η is opposite to σ. This indicates that the ability of L2 and electron transfer is higher than that of L1, indicating that electron transfer between L2 and metallic iron is easier.

ΔN_{max} is a measure of the amount of electrons that the corrosion inhibitor molecules can transfer to the metal surface. As shown in Table 5, ΔN_{max} L2>L1 indicates that L2 has a larger electron transfer capacity, which is consistent with the experimental results.

Table 5. Quantum chemical parameters of molecular structures of L1 and L2

Molecule	μ(Debye)	E_{HOMO} (eV)	E_{LUMO} (eV)	ΔE_{gap} (eV)	H	σ	ΔN_{max}
L1	2.07	-0.21813	-0.04715	4.55	2.326183	0.4298	4.197753
L2	2.96	-0.26560	-0.10357	3.51	1.755181	0.5697	5.535909

(4) Quantitative structure-activity relationship study

Quantitative structure-activity relationship (QSAR) is a quantitative study of the relationship between small organic molecules and their activities by mathematical and statistical means by means of physicochemical properties or structural parameters of molecules. QSAR has a wide range of applications in medicines, pesticides, and biological activities [47].

Through the structural parameters of the two kinds of diamine double Schiff base inhibitors in Table 5 and the inhibition rate η_w obtained by the weight loss method, the SPSS software was used for the correlation analysis, and the variables with the correlation coefficient greater than 0.3 were selected, such as the maximum transfer of chemical reactions. The electron number ΔN_{max}, the lowest unoccupied orbital energy E_{LUMO}, the highest occupied orbital energy E_{HOMO}, and the gap energy ΔE_{gap} are used as independent variables for the construction of the QSAR model. Structural parameters are correlated with experimental inhibition efficiency by establishing a quantitative structure-activity relationship model.

The QSAR model strongly relies on the adsorption mechanism of the corrosion inhibitor on the metal surface. Linear multivariate stepwise regression methods are often used when the adsorption on

the metal surface obeys the Langmuir isotherm [48]. Based on this, the quantitative structure-activity relationship model of the diamine double Schiff base corrosion inhibitor L1~L2 was established as follows:

$$\eta w\% = 364.254 + 5.488\Delta N_{max} - 197.039 E_{LUMO} + 657.110 E_{HOMO} - 35.699\Delta E_{gap} \quad (17)$$

Among them, the linear multivariate stepwise regression equation (17) has a correlation coefficient r^2 of 0.995, the significance test F is 16.380, and the residual mean square error σ^2 is 6.679. Both the regression equation and the regression coefficient pass the significance test of 0.05, indicating that the effect of ΔN_{max}, E_{LUMO}, E_{HOMO}, $\triangle E_{gap}$ on the corrosion inhibition rate is credible at a significance level of 0.05. In general, the value of r^2 is in the range of 0.873-1.00, indicating that the equation has a good linear correlation [49]. From the results of r^2, F and σ^2 in formula (17), the linear correlation between the selected four parameters and the inhibition rate of L1-L2 corrosion inhibitor is good and statistically significant. It can be seen from equation (17) that the maximum electron transfer number ΔN_{max} and the highest occupied molecular orbital energy E_{HOMO} are positively correlated with the inhibition rate η, while the lowest unoccupied orbital energy E_{LUMO} and the gap energy ΔE_{gap} and the inhibition rate η are negative relationship.

4. CONCLUSION

1. Weight loss method, polarization curve, electrochemical impedance, and SEM showed that the inhibition efficiency of diamine double Schiff base corrosion inhibitor was related to concentration. Diamine Schiff base L1 and L2 Steel has good corrosion inhibition performance to carbon in $1 mol \cdot L^{-1}$ sulfuric acid solution corrosion system.

2. Adsorption isotherms and thermodynamic parameters show that L1 and L2 molecules spontaneously adsorb on the surface of carbon steel, following the Langmuir adsorption isotherm, adsorption is an exothermic process, and cooling is beneficial to the adsorption process.

3. The results of quantum chemical structure analysis show that L1 and L2 have smaller gap energy and higher dipole moment, indicating that the corrosion inhibitor molecules can easily combine electrons with metallic iron to form strong adsorption on the surface of carbon steel.

4. The quantitative structure-activity relationship model was established by the linear multivariate stepwise regression method. The model shows that ΔN_{max} and E_{HOMO} are positively correlated with corrosion inhibition rate, while E_{LUMO} and ΔE_{gap} are negatively correlated with corrosion inhibition rate.
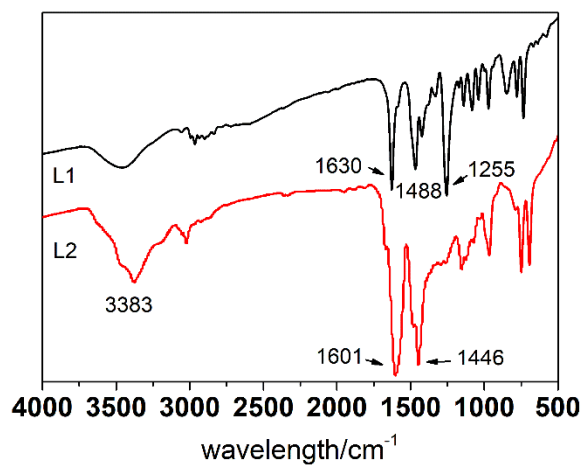
SUPPLEMENTARY DATA

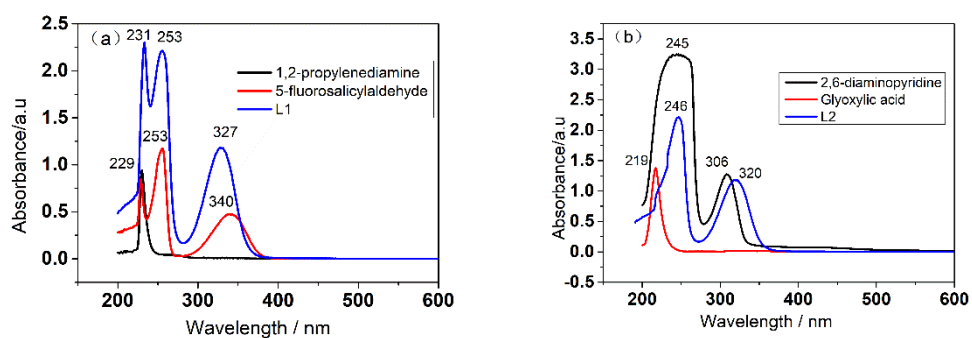**Figure S1.** Infrared spectrum of corrosion inhibitor L1 and L2

Figure S2. UV absorption spectrum of L1 and raw materials (a), L2 and raw materials (b)
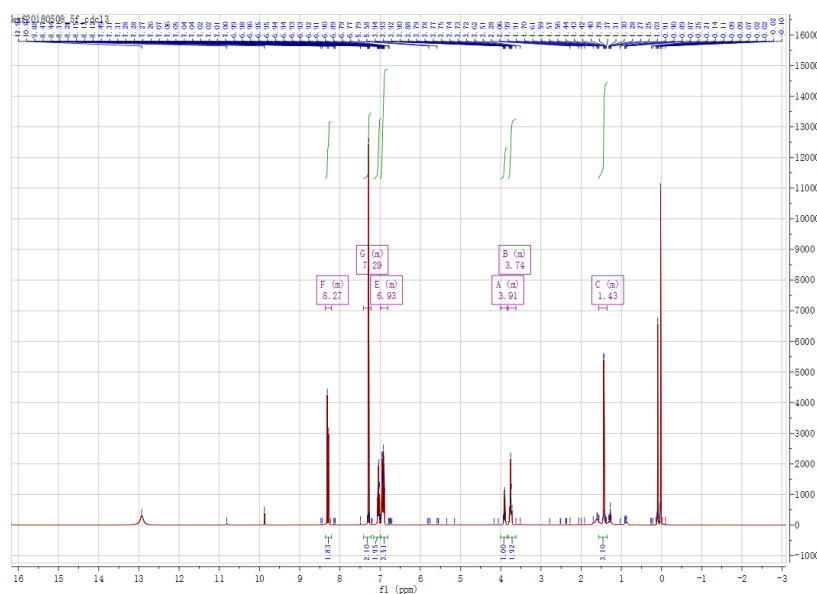
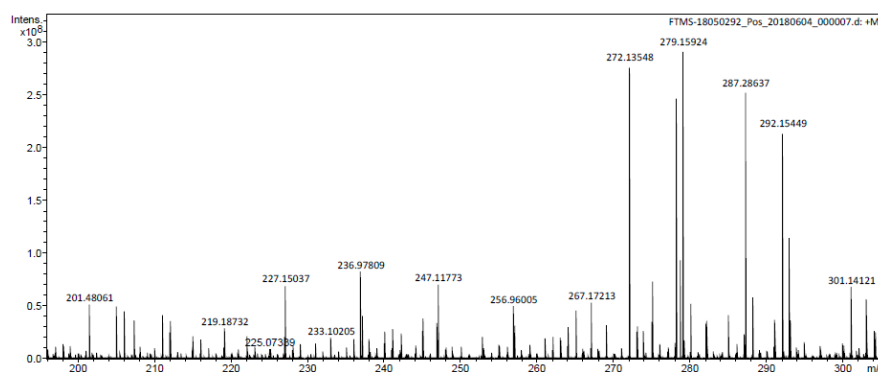

Figure S3. H-NMR spectrum of L1

Figure S4. The mass spectra of L2

References

1. J. Sebhaoui, Y. El Bakri, Y. El Aoufir, E. Anouar, A. Guenbour, A. A. Nasser, and E. Essassi, *J. Mol. Struct.,* 1182 (2019) 123.
2. J.W. Ding, B. Tang, M. Y. Li, X. F. Feng, F. L. Fu, L. Y. Bin, S. S. Huang, W. Su, D. N. Li, and L. C. Zheng, *J. Cleaner Prod*., 142 (2017) 2166.
3. H. Debab, T. Douadi, D. Daoud, S. Issaadi, and S. Chafaa, *Int. J. Electrochem. Sci.,* 13 (2018) 6958.
4. B. R. Zhang, C. J. He, C. Wang, P. D. Sun, F. T. Li, and Y. Lin, *Corros. Sci.,* 94 (2015) 6.
5. S. W. Xie, Z. Liu, G. C. Han, W. Li, J. Liu, and Z. C. Chen, *Comput. Theor. Chem*., 1063 (2015) 50.
6. S. Dehghanpour, M. Khalaj, and A. Mahmoudi, *Inorg. Chem. Commun.,* 12 (2009) 231.
7. G. Khan, W. J. Basirun, S. N. Kazi, P. Ahmed, L. Magaji, S. M. Ahmed, G. M. Khan, and M. A. Rehman, *J. Colloid Interface Sci.,* 502 (2017) 134.
8. Y. Meng, W. B. Ning, B. Xu, W. Z. Yang, K. G. Zhang, Y. Chen, L. H. Li, X. Liu, J. H. Zheng, and Y. M. Zhang, *RSC Adv.,* 7 (2017) 43014.
9. E. E. Elemike, D. C. Onwudiwe, H. U. Nwankwo, and E. C. Hosten, *J. Mol. Struct.,* 1136 (2017) 253.
10. H. Lgaz, A. Chaouiki, M. R. Albayati, R. Salghi, Y. El Aoufir, I. H. Ali, M. I. Khan, S. K. Mohamed, and I. M. Chung, *Res. Chem. Intermed.,* 45 (2019) 2269.
11. H. Keles, D. M. Emir, and M. Keles, *Corros. Sci.,* 101 (2015) 19.
12. M. Behpour, N. Mohammadi, and E. Alian, *J. Iron Steel Res. Int.,* 21 (2014) 121.
13. V. V. Torres, R. S. Amado, C. F. de Sa, T. L. Fernandez, C. A. D. Riehl, A. G. Torres, and E. D'Elia, *Corros. Sci.,* 53 (2011) 2385.
14. F. Tezcan, G. Yerlikaya, A. Mahmood, and G. Kardas, *J. Mol. Liq.,* 269 (2018) 398.
15. R. G. Pearson, *J. Am. Chem. Soc.,* 85 (1963) 3533.
16. A. Miodek, E. M. Regan, N. Bhalla, N. A. E. Hopkins, S. A. Goodchild, and P. Estrela, *Sensors-Basel.,* 15 (2015) 25015.
17. B. Ramaganthan, M. Gopiraman, L. O. Olasunkanmi, M. M. Kabanda, S. Yesudass, I. Bahadur, A. S. Adekunle, I. B. Obot, and E. E. Ebenso, *RSC Adv.,* 5 (2015) 76675.
18. K. R. Ansari, M. A. Quraishi, and A. Singh, *Corros. Sci.,* 79 (2014) 5.
19. D. B. Hmamou, A. Zarrouk, R. Salghi, H. Zarrok, E. E. Ebenso, B. Hammouti, M. M. Kabanda, N. Benchat, and O. Benali, *Int. J. Electrochem. Sci.,* 9 (2014) 120.
20. M. Wang, J. Zhang, Q. H. Wang and M. Dui, *Int J Electrochem Sci*., 14 (2019) 8852.
21. A. A. Abdulridha, M. A. A. H. Allah, S. Q. Makki, Y. Sert, H. E. Salman and A. A. Balakit, *J Mol Liq*, 315 (2020) 113690.
22. O. Moumeni, S. Chafaa, R. Kerkour, K. Benbouguerra and N. Chafai, *J. Mol. Struct*., 1206 (2020)

127693.

23. F. Chioma, C. U. Ibeji and O. Okpareke, *J. Mol. Struct.,* 1210 (2020) 128017.
24. M. M. Khalaf, A. H. Tantawy, K. A. Soliman and H. M. Abd El-Lateef, *J. Mol. Struct.,* 1203 (2020) 127442.
25. A. M. Elsharif, S. A. Abubshait, I. Abdulazeez and H. A. Abubshait, *J Mol Liq*, 319 (2020) 114162.
26. P. Singh, E. E. Ebenso, L. O. Olasunkanmi, I. B. Obot, and M. A. Quraishi, *J. Phys. Chem. C.,* 120 (2016) 3408.
27. N. K. Gupta, C. Verma, M. A. Quraishi, and A. K. Mukherjee, *J. Mol. Liq.,* 215 (2016) 47.
28. R. Yıldız, *Corros. Sci.,* 90 (2015) 544.
29. F. Tezcan, G. Yerlikaya, A. Mahmood, and G. Kardas, *J. Mol. Liq.,* 269 (2018) 398.
30. C.H. Hsu, and F. Mansfeld, *Corros. Sci.,* 57 (2001) 747.
31. J. Aljourani, K. Raeissi, and M. A. Golozar, *Corros. Sci.,* 51 (2009) 1836.
32. R. Solmaz, G. Kardas, M. Culha, B. Yazici, and M. Erbil, *Electrochim. Acta.,* 53 (2008) 5941.
33. R. Solmaz, *Corros. Sci.,* 52 (2010) 3321.
34. C. Verma, L. O. Olasunkanmi, I. B. Obot, E. E. Ebenso, and M. A. Quraishi, *RSC Adv.,* 6 (2016) 53933.
35. O. Benali, L. Larabi, M. Traisnel, L. Gengembre, and Y. Harek, *Appl. Surf. Sci.,* 253 (2007) 6130.
36. Y. P. Khodyrev, E. S. Batyeva, E. K. Badeeva, E. V. Platova, L. Tiwari and O. G. Sinyashin, *Corros. Sci.,* 53 (2011) 976.
37. E. E. Oguzie, Y. Li, and F. H. Wang, *J. Colloid Interface Sci.,* 310 (2007) 90.
38. P. C. Okafor, and Y. G. Zheng, *Corros. Sci.,* 51 (2009) 850.
39. I. B. Obot, and N. O. Obi-Egbedi, *E-J. Chem.,* 7 (2010) 837.
40. A. M. Abdel-Gaber, B. A. Abd-El-Nabey, I. M. Sidahmed, A. M. El-Zayady, and M. Saadawy, *Corros. Sci.,* 48 (2006) 2765.
41. P. C. Okafor, C. B. Liu, X. Liu, Y. G. Zheng, F. Wang, C. Y. Liu, and F. Wang, *J. Solid State Electrochem.,* 14 (2010) 1367.
42. S. A. Ali, M. T. Saeed, and S. U. Rahman, *Corros. Sci.,* 45 (2003) 253.
43. M. S. Kumar, S. L. A. Kumar, and A. Sreekanth, *Ind. Eng. Chem. Res.,* 51 (2012) 5408.
44. M. A. Quraishi, and J. Rawat, *Mater. Chem. Phys.,* 73 (2002) 118.
45. C. Verma, M. A. Quraishi, and E. E. Ebenso, *Int. J. Electrochem. Sci.,* 8 (2013) 7401.
46. K. G. Zhang, B. Xu, W. Z. Yang, X. S. Yin, Y. Liu, and Y. Z. Chen, *Corros. Sci.,* 90 (2015) 284.
47. J. Li, Y. Gao, S. Shang, X. Rao, J. Song, and Z. Wang, *RSC Adv.,* 4 (2014) 58190.
48. A. El Assyry, B. Benali, B. Lakhrissi, M. El Faydy, M. E. Touhami, R. Touir, and M. Touil, *Res. Chem. Intermed.,* 41 (2015) 3419.
49. G. Ji, S. K. Shukla, P. Dwivedi, S. Sundaram, and R. Prakash, *Ind. Eng. Chem. Res.,* 50 (2011) 11954.